RSC Advances

RSC Publishing

PAPER

View Article Online
View Journal | View Issue

Published on 24 September 2013. Downloaded by University of Western Ontario on 31/10/2014 13:25:59.

Cite this: *RSC Adv.*, 2013, **3**, 21797

Reversible Friedel–Crafts acyl rearrangements of planar polycyclic aromatic ketones: dibenzofluorenones†

Tahani Mala'bi, Sergey Pogodin, Shmuel Cohen and Israel Agranat*

Received 9th July 2013
Accepted 5th September 2013

DOI: 10.1039/c3ra43483d

www.rsc.org/advances

Dibenzofluorenones undergo reversible Friedel–Crafts acyl rearrangements in PPA at elevated temperatures. The Friedel–Crafts acyl rearrangements of 13*H*-dibenzo[*a*,*i*]fluoren-13-one (**DB*ai*F**) yield both 13*H*-dibenzo[*a*,*h*]fluoren-13-one (**DB*ah*F**) and 12*H*-dibenzo[*b*,*h*]fluoren-12-one (**DB*bh*F**). **DB*ah*F** and **DB*bh*F** undergo reversible mutual isomerizations, and their ratio depends on the reaction conditions. The *O*-protonate **DB*ah*FH$^+$** plays a pivotal role in the proposed mechanism of the reversible Friedel–Crafts acyl rearrangements. **DB*ah*FH$^+$** may undergo proton migration to give two isomeric σ-complexes: **σ-13*aH*-DB*ah*F$^+$** and **σ-12*aH*-DB*ah*F$^+$**, leading, *via* the respective naphthyl naphthoylium ions **βCOβN-βN$^+$** and **αCOβN-βN$^+$** to *O*-protonates **DB*bh*FH$^+$** and **DB*ai*FH$^+$**, respectively. The regioselectivity of the rearrangement is expressed by the preferred intramolecular *beta*-electrophilic attack in **βCOβN-βN$^+$** and by the preferred *alpha*-electrophilic attack in **αCOβN-βN$^+$**, which indicates a thermodynamic control. The proposed mechanism is supported by the results of the DFT calculations of the dibenzofluorenones, their *O*-protonates, their σ-complexes and their corresponding naphthyl naphthoylium ions at B3LYP/6-311++G(d,p). **DB*ah*F** and **DB*ai*F** are the kinetically controlled products of the Friedel–Crafts acyl rearrangement, while **DB*bh*F** is the thermodynamically controlled product. The aromaticity/antiaromaticity notions in dibenzofluorenones and their *O*-protonates, estimated by calculated HOMA and NICS indices, are discussed.

Introduction

Friedel–Crafts acylation is considered a corner stone of organic chemistry.[1] In 1955, Gore introduced the concept of reversibility of Friedel–Crafts acylation, proposing that "The Friedel–Crafts acylation reaction of reactive aromatic hydrocarbons is a reversible process".[2] Gore concluded that "Reversibility is an important factor in acylation reactions".[2] In 1973, the authoritative monograph *Friedel–Crafts Chemistry* stated that "acylation differs from alkylation in being virtually irreversible".[3] For many years it has been accepted that Friedel–Crafts acylations are usually free of rearrangements and isomerizations. The difference in behavior between Friedel–Crafts acylation and Friedel–Crafts alkylation was attributed to the resonance stabilization existing between the acyl group and the aromatic nucleus,[4] which may serve as a barrier against rearrangements and reversible processes. The pattern of irreversibility of Friedel–Crafts acylation has been violated when the acyl group was tilted out of the plane of the aromatic nucleus, *e.g.*, by neighboring bulky substituents.[4,5] Under such a scenario, deacylations and acyl rearrangements have become feasible.[6] The reversibility studies have been focused mainly on unusual aspects of selectivity, including deacylations, uni-directional rearrangements and kinetic control *versus* thermodynamic control.[6] The pattern of irreversibility of Friedel–Crafts acylations has been highlighted under classical experimental conditions, ($AlCl_3$, a trace of water) *e.g.*, in the naphthalene series.[6–8]

The incursion of reversibility in Friedel–Crafts acylation was revealed in 1974 by Agranat *et al.* in the benzoylation of naphthalene in polyphosphoric acid (PPA) at elevated temperatures.[9] The kinetically controlled 1-benzoylnaphthalene rearranged to the thermodynamically controlled 2-benzoylnaphthalene (PPA, 140 °C), whereas the latter underwent only deacylation to give naphthalene. The reversibility concept was then applied to the synthesis of linearly annelated polycyclic aromatic ketones (PAKs) by intramolecular Friedel–Crafts acyl rearrangements of their angularly annelated constitutional isomers.[10–12] Complete reversibility of Friedel–Crafts acylation was established in the *para* ⇌ *ortho* acyl rearrangement of fluorofluorenones in PPA.[13] Further experimental evidence in support of true reversibility of Friedel–Crafts acylations and acyl rearrangements is limited.[14–23] The relative contribution of kinetic control *versus* thermodynamic control in Friedel–Crafts acyl rearrangements remains an open question, in spite of the rich chemistry of Friedel–Crafts

Organic Chemistry, Institute of Chemistry, The Hebrew University of Jerusalem, Philadelphia Bldg. #201/205, Edmond J. Safra Campus, Jerusalem 91904, Israel. E-mail: isri.agranat@mail.huji.ac.il

† Electronic supplementary information (ESI) available: ^{1}H- and ^{13}C-NMR spectra of **DB*ai*F**, **DB*ah*F**, **DB*bh*F** and **DB*cg*F**; crystallographic data for compounds **DB*ah*F**, **DB*ai*F** and **DB*cg*F**; Cartesian coordinates, total and relative B3LYP/6-311++G(d,p) energies, selected geometric parameters, HOMA and NICS indices of dibenzofluorenones, their *O*-protonates, σ-complexes and naphthyl naphthoylium ions. CCDC 920378 and 920382. For ESI and crystallographic data in CIF or other electronic format see DOI: 10.1039/c3ra43483d

Published on 24 September 2013. Downloaded by University of Western Ontario on 31/10/2014 13:25:59.

acylations.[1,24] We have recently reported that kinetic control wins out over thermodynamic control in the Friedel–Crafts acyl rearrangements of diacetylanthracenes in PPA.[25] The conformational variations in these PAKs, which contribute to the understanding of the motifs of reversibility, have been described.[26]

We report here the results of experimental and theoretical study of the intramolecular Friedel–Crafts acyl rearrangements of dibenzofluorenones in PPA. We highlight the reversibility characteristics and the preference of thermodynamic control in the acyl rearrangements of these planar PAKs and the relevance of the notions of aromaticity/antiaromaticity herein.

Results and discussion

Eleven constitutional isomers of dibenzofluorenone under study are shown in Fig. 1. The following dibenzofluorenones, benzologs of 9*H*-fluoren-9-one (**Fl**), were considered in the present study: 13*H*-dibenzo[*a*,*i*]fluoren-13-one (**DB*ai*F**), 13*H*-dibenzo[*a*,*h*]fluoren-13-one (**DB*ah*F**), 12*H*-dibenzo[*b*,*h*]fluoren-12-one (**DB*bh*F**), 13*H*-dibenzo[*a*,*g*]fluoren-13-one (**DB*ag*F**), 7*H*-dibenzo[*b*,*g*]fluoren-7-one (**DB*bg*F**), and 7*H*-dibenzo[*c*,*g*]fluoren-7-one (**DB*cg*F**). The remaining constitutional isomers of dibenzofluorenone (in Fig. 1), *i.e.* dibenzo[*a*,*c*]fluoren-13-one (**DB*ac*F**, aka 13*H*-indeno[1,2-*l*]phenanthrene), 7*H*-benzo[*hi*]chrysen-13-one (**B*hi*C**), 7*H*-benzo[*de*]naphthacen-7-one (**B*de*NC**), 7*H*-dibenzo[*a*,*kl*]anthracen-7-one (**DB*akl*AN**) and 7*H*-benzo[*ij*]pleiaden-7-one (**B*ij*P**) were outside the scope of the present study. We have focused our attention on the Friedel–Crafts acyl rearrangements of **DB*ai*F**, **DB*ah*F** and **DB*bh*F**. The reported study includes synthesis, X-ray crystallography, ^{1}H- and ^{13}C-NMR spectroscopy, acyl rearrangements and DFT calculations.

The names of dibenzofluorenones imply dibenzo[*a*,*i*]-, [*a*,*h*]-, [*b*,*h*]-, [*a*,*g*]-, [*b*,*g*]- or [*c*,*g*]-annelation of the parent fluorenone system. Dibenzofluorenones may be perceived as bridged dinaphthyl ketones. **DB*ai*F** is a bridged 1*Z*,1*Z*′-dinaphthyl ketone (**11′DN**); **DB*ah*F** is a bridged 1*Z*,2*Z*′-dinaphthyl ketone (**12′DN**); **DB*bh*F** is a bridged 2*Z*,2*Z*′-dinaphthyl ketone (**22′DN**); **DB*ag*F** is a bridged 1*Z*,2*E*′-dinaphthyl ketone; **DB*bg*F** is a bridged 2*Z*,2*E*′-dinaphthyl ketone; **DB*cg*F** is a bridged 2*E*,2*E*′-dinaphthyl ketone. However, contrary to the dinaphthyl ketones which are non planar,[27] the dibenzofluorenones, except **DB*cg*F**, are planar (*vide infra*).

Synthesis and NMR spectroscopy

All the dibenzofluorenones under study have been described in the literature. **DB*ai*F** was synthesized according to a literature procedure[27] by oxidation of 13*H*-dibenzo[*a*,*i*]fluorene, formed by acid cyclodehydration of di-1-naphthyl methanol. **DB*bh*F** was synthesized according to a literature procedure[28] by a double aldol condensation of benz[*f*]indan-1-one and *o*-phthaldialdehyde in MeOH/KOH. **DB*ah*F**[29,30] was synthesized in the present study by PPA mediated acyl rearrangement of **DB*ai*F** (*vide infra*). **DB*cg*F** was prepared according to a literature procedure[31] by decarboxylation of [1,1′-binaphthalene]-2,2′-dicarboxylic acid, obtained from 1-bromo-2-naphthoic acid.

The structures of **DB*ai*F**, **DB*ah*F** and **DB*bh*F** have been verified by ^{1}H-NMR and ^{13}C-NMR spectroscopies (*vide infra*). The structure of **DB*ah*F** has also been verified by X-ray crystallography (*vide infra*). Table 1 gives the experimental ^{1}H-NMR chemical shifts of **DB*ai*F**, **DB*ah*F** and **DB*bh*F** and of their *O*-protonates. Table 2 gives the ^{13}C-NMR chemical shifts of **DB*ai*F**, **DB*ah*F** and **DB*bh*F** and of their *O*-protonates. Complete assignments were made through 2-dimensional correlation spectroscopy (DQF-COSY, HSQC, and HMBC).

We note the deshielding of the protons (in $CDCl_3$) very close to the carbonyl group in **DB*ai*F** and **DB*ah*F**: $\delta(H^1, H^{12}) = 8.95$ ppm (**DB*ai*F**) and $\delta(H^1) = 9.13$ ppm (**DB*ah*F**), as compared with the protons *peri* to the carbonyl, $\delta(H^{12}) = 8.14$ ppm (**DB*ah*F**) and $\delta(H^{11}, H^{13}) = 8.27$ ppm (**DB*bh*F**). The deshielding of the carbonyl carbon is also noted: $\delta(^{13}C{=}O)$(**DB*ai*F**)–$\delta(^{13}C{=}O)$(**DB*ah*F**) = 3.4 ppm and $\delta(^{13}C)$(**DB*ai*F**)–$\delta(^{13}C)$(**DB*bh*F**) = 4.8 ppm. These relative downfield shifts indicate contributions of dipolar structures with partial positive charges on the carbonyl carbon atoms in the order **DB*ai*F** > **DB*ah*F** > **DB*bh*F**. The same order, but a smaller effect is indicated in the mixture of trifluoroacetic acid : $CDCl_3$ (19 : 1): $\delta(^{13}C{=}O)$(**DB*ai*F**)–$\delta(^{13}C{=}O)$(**DB*ah*F**) = 2.2 ppm and $\delta(^{13}C{=}O)$(**DB*ai*F**)–$\delta(^{13}C{=}O)$(**DB*bh*F**) = 3.2 ppm. In this media dibenzofluorenones exists in the form of *O*-protonates: **DB*ai*FH$^+$**, **DB*ah*FH$^+$** and **DB*bh*FH$^+$** (*vide infra*).

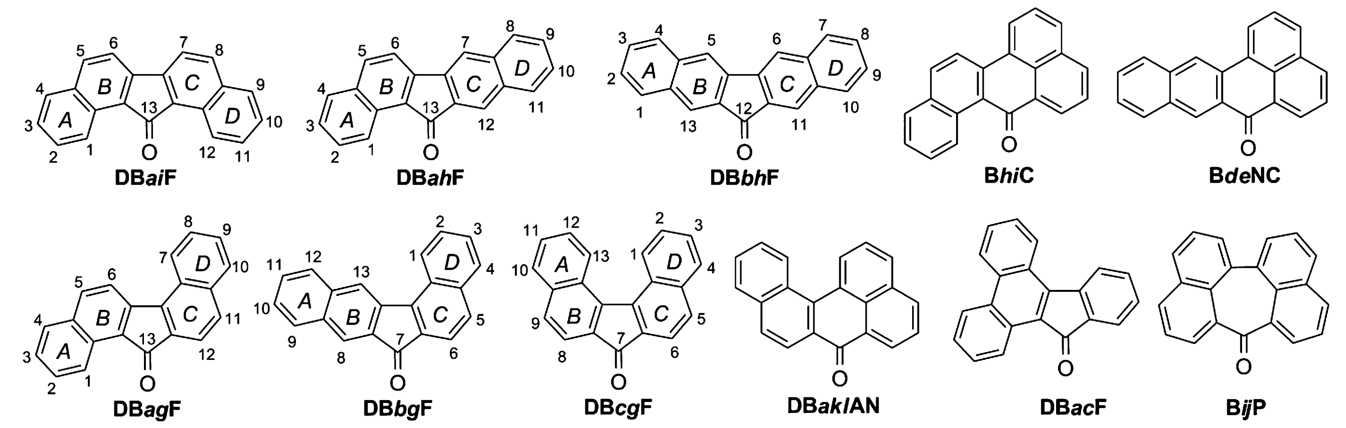

Fig. 1 Isomeric $C_{21}H_{12}O$ PAKs.

Published on 24 September 2013. Downloaded by University of Western Ontario on 31/10/2014 13:25:59.

Table 1 ^{1}H-NMR chemical shifts (δ, ppm) of **DB*ai*F**, **DB*ah*F** and **DB*bh*F** (in $CDCl_3$) and of their *O*-protonates (in TFA : $CDCl_3$ 19 : 1)

	δ(DB*ai*F)	δ(DB*ai*FH$^+$)	Δδ(DB*ai*F–DB*ai*FH$^+$)	δ(DB*ah*F)	δ(DB*ah*FH$^+$)	Δδ(DB*ah*F–DB*ah*FH$^+$)	δ(DB*bh*F)	δ(DB*bh*FH$^+$)	Δδ(DB*bh*F–DB*bh*FH$^+$)
H^1	8.95	8.56	0.39	9.13	8.64	0.49	7.92	7.65	0.27
H^2	7.57	7.56	0.01	7.66	7.48	0.18	7.49	7.37	0.12
H^3	7.41	7.39	0.02	7.51	7.36	0.15	7.57	7.50	0.07
H^4	7.76	7.74	0.02	7.84	7.60	0.26	7.88	7.70	0.18
H^5	7.96	7.97	−0.01	8.08	7.80	0.28	8.09	7.78	0.31
H^6	7.66	7.60	0.06	7.85	7.44	0.41	8.09	7.78	0.31
H^7	7.66	7.60	0.06	7.86	7.41	0.45	7.88	7.70	0.18
H^8	7.96	7.97	−0.01	7.85	7.55	0.30	7.57	7.50	0.07
H^9	7.76	7.74	0.02	7.56	7.42–7.43	0.14	7.49	7.37	0.12
H^{10}	7.41	7.39	0.02	7.49	7.32	0.17	7.92	7.65	0.27
H^{11}	7.57	7.56	0.01	7.91	7.56	0.36	8.27	7.96	0.31
H^{12}	8.95	8.56	0.39	8.14	7.65	0.49	—	—	—
H^{13}	—	—	—	—	—	—	8.27	7.96	0.31

In the *O*-protonates, the protons close to the carbonyl group exhibit considerable upfield shifts relative to those in the parent ketones: $\Delta\delta(^{1}H) = 0.39$ ppm (H^1, H^{12}, **DB*ai*FH$^+$**), 0.49 ppm (H^1, H^{12}, **DB*ah*FH$^+$**), 0.31 ppm (H^{11}, H^{13}, **DB*bh*FH$^+$**). The carbonyl carbons in the *O*-protonates are shifted downfield relative to those in the parent ketones: $\Delta\delta(^{13}C) = -5.9$ ppm (C^{13}, **DB*ai*FH$^+$**), −7.1 ppm (C^{13}, **DB*ah*FH$^+$**), −7.5 ppm (C^{12}, **DB*bh*FH$^+$**).

Molecular and crystal structures

The molecular and crystal structures of **DB*ai*F**[33] and **DB*cg*F**[34] have previously been reported. The molecular and crystal structures of **DB*ah*F** and **DB*cg*F** are reported here.[32] PAK **DB*ah*F** crystallizes in the monoclinic space group $P2_1/c$ with unit cell dimensions $a = 13.3493$, $b = 7.6721$, $c = 13.0564$ Å, and $\beta = 94.888°$. PAK **DB*cg*F** crystallizes in the orthorhombic space group $P2_1/n$ with unit cell dimensions $a = 16.753$, $b = 14.395$, $c = 5.793$ Å, and $\beta = 91.0°$. Fig. 2 and 3 depict ORTEP diagrams of **DB*ah*F** and **DB*cg*F** respectively, as determined by X-ray analysis (anisotropic displacement parameters are drawn at the 50% probability level). The crystallographic data of **DB*ah*F**, **DB*cg*F** and **DB*ai*F** are given in Table S1 in the ESI.†

Table 3 gives selected structural parameters derived from the crystal structures of **DB*ah*F**, **DB*ai*F** and **DB*cg*F**. The most

Table 2 ^{13}C-NMR chemical shifts (δ, ppm) of **DB*ai*F**, **DB*ah*F** and **DB*bh*F** (in $CDCl_3$) and of their *O*-protonates (in TFA : $CDCl_3$ 19 : 1)

	δ(DB*ai*F)	δ(DB*ai*FH$^+$)	Δδ(DB*ai*F–DB*ai*FH$^+$)	δ(DB*ah*F)	δ(DB*ah*FH$^+$)	Δδ(DB*ah*F–DB*ah*FH$^+$)	δ(DB*bh*F)	δ(DB*bh*FH$^+$)	Δδ(DB*bh*F–DB*bh*FH$^+$)
C^1	124.0	125.5	−1.5	124.7	126.3	−1.6	130.8	133.2	−2.3
C^2	129.4	132.2	−2.8	129.5	132.5	−3.0	126.9	129.5	−2.6
C^3	126.2	128.6	−2.5	126.8	129.4	−2.6	129.1	132.3	−3.2
C^4	128.6	131.1	−2.6	128.6	131.2	−2.6	128.7	130.8	−2.1
C^{4a}	134.8	137.5	−2.7	134.3	136.9	−2.6	137.3	140.3	−3.0
C^5	135.3	139.1	−3.8	136.3	141.0	−4.7	119.7	122.1	−2.4
C^{5a}	—	—	—	—	—	—	138.8	140.7	−1.8
C^{5b}	—	—	—	—	—	—	138.8	140.7	−1.8
C^6	117.9	120.3	−2.4	118.5	120.6	−2.1	119.7	122.1	−2.4
C^{6a}	145.4	148.8	−3.4	146.5	150.9	−4.4	137.3	140.3	−3.0
C^{6b}	145.4	148.8	−3.4	138.2	139.8	−1.6	—	—	—
C^7	117.9	120.3	−2.4	118.9	122.2	−3.2	128.7	130.8	−2.1
C^{7a}	—	—	—	136.8	139.7	−2.9	—	—	—
C^8	135.3	139.1	−3.8	128.9	131.3	−2.4	129.1	132.3	−3.2
C^{8a}	134.8	137.5	−2.7	—	—	—	—	—	—
C^9	128.6	131.1	−2.6	128.9	132.3	−3.4	126.9	129.5	−2.6
C^{9a}	—	—	—	—	—	—	—	—	—
C^{10}	126.2	128.6	−2.5	127.0	129.9	−2.9	130.8	133.2	−2.3
C^{10a}	—	—	—	—	—	—	133.7	135.6	−1.9
C^{11}	129.4	132.2	−2.8	130.9	133.4	−2.6	125.7	129.9	−4.2
C^{11a}	—	—	—	134.0	136.2	−2.2	134.3	135.0	−0.7
C^{12}	124.0	125.5	−1.5	125.1	129.4	−4.3	192.8	200.3	−7.5
C^{12a}	130.2	132.6	−2.4	133.5	134.7	−1.2	134.3	135.0	−0.7
C^{12b}	126.8	128.9	−2.2	—	—	—	—	—	—
C^{13}	197.6	203.5	−5.9	194.2	201.3	−7.1	125.7	129.9	−4.2
C^{13a}	126.8	128.9	−2.2	129.7	131.1	−1.4	133.7	135.6	−1.9
C^{13b}	130.2	132.6	−2.4	130.3	132.7	−2.4	—	—	

Published on 24 September 2013. Downloaded by University of Western Ontario on 31/10/2014 13:25:59.

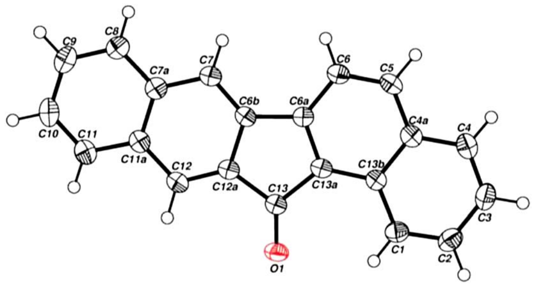

Fig. 2 ORTEP drawings of **DB*ah*F**.

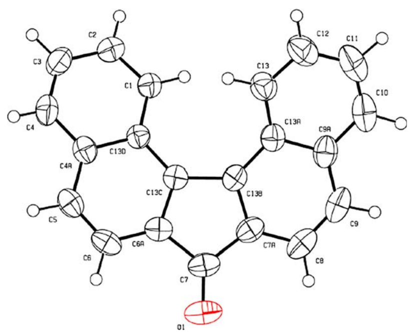

Fig. 3 ORTEP drawing of **DB*cg*F**.

important feature of the X-ray structures of **DB*ah*F** and **DB*ai*F** is their planarity, in spite of the angular monobenzo[*a*]- and dibenzo[*a*]annelation in **DB*ah*F** and **DB*ai*F**, respectively. It appears that despite the close proximity between the carbonyl oxygen and the closest aromatic hydrogen, the non-bonded C═O···H distances, which might have caused the titling of the carbonyl group from the planes of the aromatic nuclei, are larger than the sum of the Van-der-Waals radii of oxygen (129 pm) and hydrogen (115 pm).[35] It is expected that the linearly dibenzo[*b*]annelated **DB*bh*F** would also be planar. By contrast, **DB*cg*F** is not planar due to the prohibitively short non-bonded $H^1\cdots H^{13}$ distance in the "*fjord*" region, 214 pm, which causes a twist around C^{13b}–C^{13c} bond: C^{13}–C^{13a}–C^{13b}–C^{13c} = 12.2°, C^{13a}–C^{13b}–C^{13c}–C^{13d} = 22.8°. The dihedral angle between the two naphthalene nuclei in **DB*cg*F**, Φ = 27.1°, is also noted. The geometrical parameters of the molecular structures of **DB*ah*F**, **DB*ai*F** and **DB*cg*F** are in a good agreement with the respective parameters of the B3LYP/6-311++G(d,p) calculated global minima conformations of these ketones (*vide infra*).

The molecules in the crystal structures of **DB*ah*F** (Fig. 4) and **DB*cg*F** (Fig. 5) are arranged in the *herring-bone* pattern, *i.e.* in two sets of parallel planes.[36] For **DB*ah*F** the interplanar distance is 341.8 pm (between x, y, z plane and $1 - x, 1 - y, 1 - z$ plane), and non-parallel planes (x, y, z and $1 - x, 0.5 + y, 0.5 - z$) form dihedral angle of 68.7°. The molecules of **DB*ah*F** lying in the parallel planes demonstrate aromatic–aromatic $\pi\cdots\pi$ interactions, with the shortest distances between the centroids of the aromatic rings of $CgA\cdots CgD$ = 373.2 pm, $CgB\cdots CgC$ = 373.2 pm (see Fig. 1 for the numbering of the aromatic rings). The molecules lying in the non-parallel planes demonstrate C–H···π interactions, with the shortest distances between the centroids of one molecule (x, y, z plane) and the aromatic hydrogens of another molecules ($1 - x, 0.5 + y, 0.5 - z$ plane) of $H^5\cdots CgD$ = 273.2 pm, $H^6\cdots CgC$ = 275.9 pm.

For **DB*cg*F** (Fig. 5) the interplanar distances are 379.2 pm (x, y, z plane *vs.* $x, y, 1 + z$ plane) and 357.8 pm ($-0.5 + x, 0.5 - y, 0.5 - z$ plane *vs.* $1.5 - x, -0.5 + y, 1.5 - z$ plane), and the dihedral angle is 68.7° (x, y, z plane *vs.* $-0.5 + x, 0.5 - y, 0.5 - z$ plane). Both $\pi\cdots\pi$ and C–H···π intermolecular interactions in **DB*cg*F** are slightly weaker than in **DB*ah*F**. The shortest distance between the aromatic rings is $CgD\cdots CgB$ = 389.2 pm, while the shortest non-bonding C···H distance is $H^9\cdots CgA$ = 296.5 pm.

Friedel–Crafts acyl rearrangements

In the present study PAKs **DB*ai*F**, **DB*ah*F** and **DB*bh*F** were each subjected to PPA at 120–160 °C for 4–10 h. The results are summarized in Table 4. The constitution of the crude products

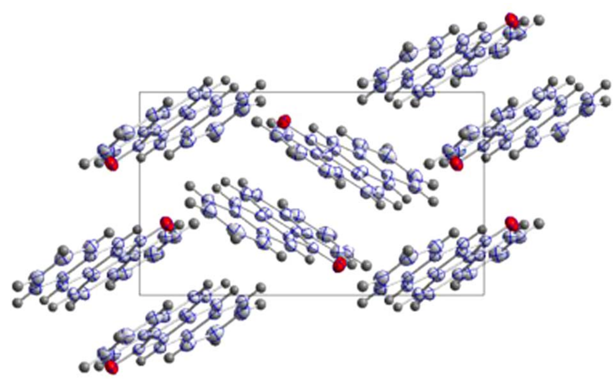

Fig. 4 The packing diagram of **DB*ah*F**, viewed down the (1, 0, 0) axis.

Table 3 Selected X-ray geometrical parameters of **DB*ah*F**, **DB*ai*F** and **DB*cg*F**

	Φ^a (deg)	χ^b (deg)	β^c (deg)	C═O (pm)	O···H^d (pm)	C···C^e (pm)	H···H^e (pm)
DB*ai*F	1.9	0.4	105.9	122.3	247.5	326.9	259.2
DB*ah*F	4.1	0.8	105.2	121.8	250.2	326.1	263.8
DB*cg*F	27.1	1.2	105.6	121.6	292.4	317.5	214.4

^{a} Dihedral angle between the least-square planes of two naphthyl moieties. ^{b} Pyramidalization angle at the carbonyl carbon is the improper torsion angles C^{12b}–C^{13}–O^1–C^{13a} (**DB*ai*F**), C^{12a}–C^{13}–O^1–C^{13a} (**DB*ah*F**) or C^{6a}–C^7–O^1–C^{7a} (**DB*cg*F**), respectively, minus 180° MOD 360. ^{c} Bond angle C^{12b}–C^{13}–C^{13a} (**DB*ai*F**), C^{12a}–C^{13}–C^{13a} (**DB*ai*F**) or C^{6a}–C^7–C^{7a} (**DB*cg*F**). ^{d} The closest distance between the oxygen and an aromatic hydrogen $O^1\cdots H^{12}$ (**DB*ai*F**), $O^1\cdots H^1$ and $O^1\cdots H^{12}$ (**DB*ah*F**), or $O^1\cdots H^6$ (**DB*cg*F**). ^{e} The non-bonding distances $C^6\cdots C^7$ and $H^6\cdots H^7$ (**DB*ai*F**, **Dbah*F**) or $C^1\cdots C^{13}$ and $H^1\cdots H^{13}$ (**DB*cg*F**).

This journal is © The Royal Society of Chemistry 2013

Published on 24 September 2013. Downloaded by University of Western Ontario on 31/10/2014 13:25:59.

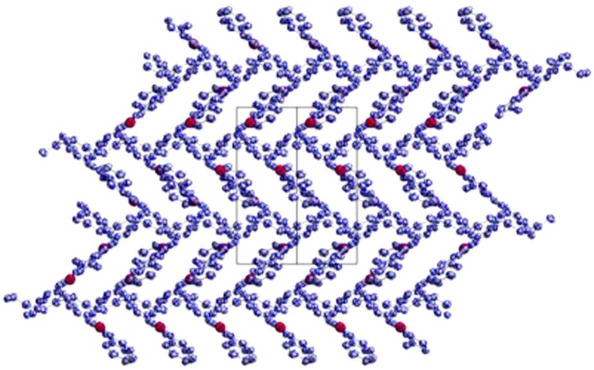

Fig. 5 The packing diagram of **DB*cg*F**, viewed down the (1,0,1) axis.

of the reactions was determined by ^{1}H-NMR spectroscopy. The constitutional isomers **DB*ai*F**, **DB*ah*F** and **DB*bh*F** were distinguished by the low-field ^{1}H-NMR chemical shifts of the protons closest to the carbonyl group: H^{1} and H^{12} (doublet) in **DB*ai*F**, H^{1} (doublet) in **DBahF** and H^{11} and H^{13} (singlet) in **DB*bh*F** (Table 1) (*vide supra*).

The Friedel–Crafts acyl rearrangements of **DB*ai*F** in PPA yield both **DB*ah*F** and **DB*bh*F**. The ratio **DB*bh*F/DB*ah*F** increases significantly (from 1 : 44 to 30 : 37) upon lengthening the reaction time and raising the reaction temperature. Preparative rearrangement of **DB*ai*F** in PPA (at 140 °C) for three hours gave **DB*ah*F** in 25% yield. **DB*ah*F** and **DB*bh*F** undergo mutual isomerization, and their ratio depends on the reaction conditions. Thus, the acyl rearrangement of the dibenzofluorenones suggests certain features of reversibility: **DB*ai*F** → **DB*ah*F** ⇌ **DB*bh*F**. Unidirectional Friedel–Crafts acyl rearrangement of 11*H*-benzo[*a*]fluoren-11-one to 11*H*-benzo[*b*]fluoren-11-one in PPA has briefly been reported.[11]

A plausible mechanism of the Friedel–Crafts acyl rearrangements of the dibenzofluorenones in PPA is presented in Scheme 1. The proposed mechanism of the consecutive rearrangements **DB*ai*F** → **DB*ah*F** ⇌ **DB*bh*F** includes formation of their respective *O*-protonates, σ-complexes and naphthyl naphthoylium ions. It involves the following steps:

Table 4 Products of Friedel–Crafts acyl rearrangements of **DB*ai*F**, **DB*ah*F** and **DB*bh*F**

Starting isomers	Temp (°C)	Reaction time (h)	Products (% relative yield)		
			DB*ai*F	**DB*ah*F**	**DB*bh*F**
DB*ai*F	140	3	55	44	1
DB*ai*F	140	5	54	42	4
DB*ai*F	140	8	52	34	14
DB*ai*F	160	8	33	37	30
DB*ai*F	160	10	9	43	48
DB*ah*F	120	4	0	97	3
DB*ah*F	140	6	0	76	23
DB*ah*F	160	6	0	58	42
DB*ah*F	160	10	0	60	40
DB*bh*F	140	5	0	9	91
DB*bh*F	140	8	0	34	66
DB*bh*F	160	6	0	28	72

(i) protonation of **DB*ai*F** to give the *O*-protonate **DB*ai*FH^{+}**;

(ii) proton migration to give the σ-complex **σ-12*bH*-DB*ai*F^{+}**;

(iii) 5-membered-ring cleavage to give 2-(2′-naphthyl)-1-naphthoylium ion **αCOβN-βN^{+}**;

(iv) conformational isomerization of **αCOβN-βN^{+}** by rotation around the C^{2}–$C^{2'}$ bond;

(v) regioselective intramolecular acylation at $C^{3'}$ of the 2′-naphthyl substituent to give the σ-complex **σ-12*aH*-DB*ah*F^{+}**;

(vi) proton migration and rearomatization to give the *O*-protonate **DB*ah*FH^{+}**;

(vii$_{a}$) proton migration to give the more stable σ-complex **σ-13*aH*-DB*ah*F^{+}**;

(vii$_{b}$) alternatively, deprotonation of **DB*ah*FH^{+}** to give the intermediate product **DB*ah*F**;

(viii) 5-membered-ring cleavage to give 3-(2′-naphthyl)-2-naphthoylium ion **βCOβN-βN^{+}**;

(ix) conformational isomerization of **βCOβN-βN^{+}** by rotation around the C^{3}–$C^{2'}$ bond;

(x) regioselective intramolecular acylation at $C^{3'}$ of the 2′-naphthyl substituent to give the σ-complex **σ-11*aH*-DB*bh*F^{+}**;

(xi) proton migration to give the O-protonate **DB*bh*FH^{+}**;

(xii) deprotonation of **DB*bh*FH^{+}** to give the final product **DB*bh*F**.

The *O*-protonate **DB*ah*FH^{+}** plays a pivotal role in the proposed mechanism of the consecutive rearrangements. This *O*-protonate may undergo proton migration to give two isomeric σ-complexes: **σ-13*aH*-DBahF^{+}** and **σ-12*aH*-DB*ah*F^{+}**. The preferred formation of **σ-13*aH*-DB*ah*F^{+}** allows its 5-membered ring cleavage to give **βCOβN-βN^{+}** ion. An intramolecular electrophilic attack by the 2-naphthoylium ion at the *beta*-position ($C^{3'}$) of the 2′-naphthyl substituent gives the σ-complex **σ-11*aH*-DB*bh*F^{+}**, which then undergoes proton migration leading to the linearly benzo[*b*]annelated *O*-protonate **DB*bh*FH^{+}**. Alternatively, the formation of the less stable σ-complex **σ-12*aH*-DB*ah*F^{+}** would have led to **αCOβN-βN^{+}** ion, which would undergo intramolecular electrophilic attack by the 1-naphthoylium ion at the *alpha*-position ($C^{1'}$) of the 2′-naphthyl substituent to give **σ-12*bH*-DB*ai*F^{+}**. Proton migration in the latter σ-complex leads to **DB*ai*FH^{+}**. The regioselectivity is expressed in the preferred *alpha*-carbonyl cleavage of **σ-13*aH*-DBahF^{+}** followed by the intramolecular *beta*-electrophilic attack in **βCOβN-βN^{+}** over *beta*-carbonyl cleavage of **σ-12*aH*-DBahF^{+}** followed by the *alpha*-electrophilic attack in **αCOβN-βN^{+}**. The preference for *beta*-substitution over *alpha*-substitution in the Friedel–Crafts acylations of naphthalenes is indicative of a thermodynamic control (*vide infra*). The preferred pathway of the rearrangements is summarized:

DB*ai*F ⇌ DB*ai*FH^{+} ⇌ σ-12*bH*-DB*ai*F^{+} ⇌ αCOβN-βN ⇌ σ-12*aH*-DB*ah*F^{+} ⇌ DB*ah*FH^{+} ⇌ σ-13*aH*-DB*ah*F^{+} ⇌ βCOβN-βN^{+} ⇌ σ-11*aH*-DB*bh*F^{+} ⇌ DB*bh*FH^{+} ⇌ DB*bh*F.

DFT study

DFT methods are capable of generating a variety of isolated molecular properties quite accurately, especially *via* the hybrid functionals, and in a cost-effective way.[37,38] Recently, the B3LYP

Published on 24 September 2013. Downloaded by University of Western Ontario on 31/10/2014 13:25:59.

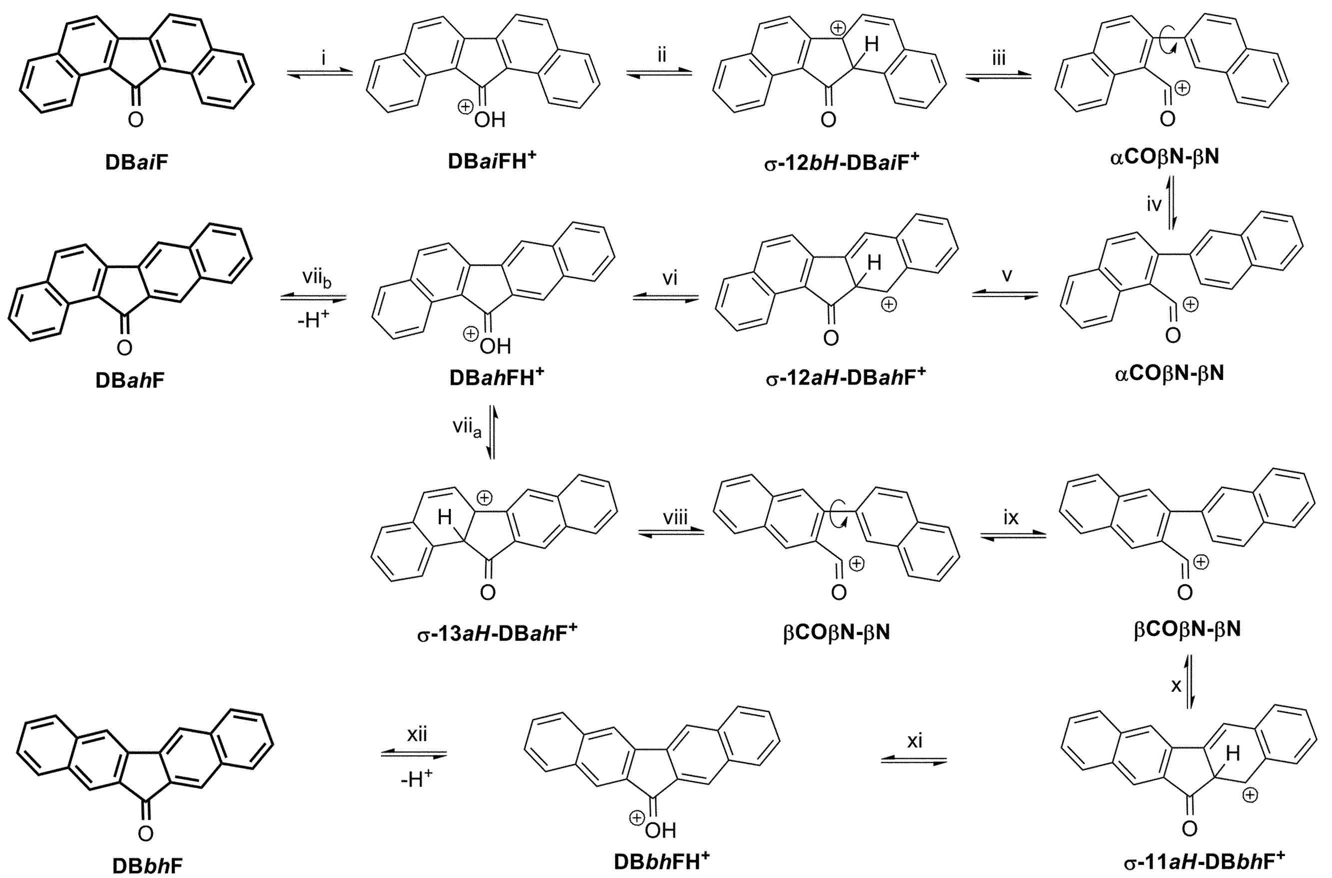

Scheme 1 Proposed mechanism of the Friedel–Crafts acyl rearrangements of dibenzofluorenones in PPA.

hybrid functional was successfully employed to treat dinaphthyl ketones, dinaphthyl thioketones and dinaphthyl diazomethanes[27] and overcrowded BAEs.[39–41] PAKs **DB*ai*F**, **DB*ah*F**, **DB*bh*F**, **DB*cg*F**, **DB*ag*F** and **DB*bg*F**, their *O*-protonates, their σ-complexes and the structurally related naphthyl naphthoylium ions were subjected to a computational DFT study. Their relative B3LYP/6-311++G(d,p) Gibbs free energies (ΔG_{298} and $\Delta\Delta G_{298}$) are presented in Table 5; total and relative energies and selected geometrical parameters are presented in the ESI (Tables S2–S5†).

Dibenzofluorenones (Fig. 1) adopt planar C_s or C_{2v} conformations, except for **DB*cg*F**, which is twisted around C^{6b}–C^{12b}: the dihedral angle between the naphthalene systems is $\Phi = 26°$; its planar C_{2v} conformer features prohibitively short $H^1 \cdots H^{13}$

Table 5 Relative B3LYP/6-311++G(d,p) free energies (ΔG_{298} and $\Delta\Delta G_{298}$, kJ mol^{-1}) of dibenzofluorenones, their respective *O*-protonates, σ-complexes and naphthyl naphthoylium ions

Ketones		ΔG_{298} ^{a}	*O*-Protonates		ΔG_{298} ^{b}	σ-Complexes		ΔG_{298} ^{b}	$\Delta\Delta G_{298}$	Naphthyl naphthoylium ions		ΔG_{298} ^{b}	$\Delta\Delta G_{298}$
DB*bh*F	C_{2v}	0.00	**DB*bh*FH$^+$**	C_s	0.00	**σ-11*aH*-DB*bh*F$^+$**	C_1	100.05	32.51	**βCOβN-βN$^+$**	C_1	81.37	13.64
DB*ah*F	C_s	1.74	**DB*ah*FH$^+$**	C_s	3.99	**σ-13*aH*-DB*ah*F$^+$**	C_1	67.54	0.00	**βCOβN-βN$^+$**	C_1	79.57	11.84
			DB*ah*FH$^+$	C_1	8.81	**σ-12*aH*-DB*ah*F$^+$**	C_1	100.84	33.29	**αCOβN-βN$^+$**	C_1	69.84	2.11
DB*bg*F	C_s	10.10	**DB*bg*FH+**	C_s	13.03	**σ-6*aH*-DB*bg*F$^+$**	C_1	97.60	30.06	**βCOβN-αN$^+$**	C_1	89.13	21.40
										βCOβN-αN$^+$		90.22	22.49
			DB*bg*FH$^+$	C_s	15.87	**σ-7*aH*-DB*bg*F$^+$**	C_1	108.62	41.08	**βCOαN-βN$^+$**	C_1	81.40	13.67
DB*ai*F	C_{2v}	16.14	**DB*ai*FH$^+$**	C_1	34.92	**σ-12*bH*-DB*ai*F$^+$**	C_1	69.26	1.71	**αCOβN-βN$^+$**	C_1	67.73	0.00
DB*ag*F	C_s	23.42	**DB*ag*FH$^+$**	C_s	39.47	**σ-13*aH*-DB*ag*F$^+$**	C_1	76.93	9.39	**βCOαN-βN$^+$**	C_1	78.81	11.08
			DB*ag*FH$^+$	C_1	47.70	**σ-12*aH*-DB*ag*F$^+$**	C_1	99.35	31.80	**αCOβN-αN$^+$**	C_1	79.05	11.32
										αCOβN-αN$^+$		84.64	16.91
DB*cg*F	C_2	55.61	**DB*cg*FH$^+$**	C_1	73.35	**σ-6*aH*-DB*cg*F$^+$**	C_1	117.90	50.36	**βCOαN-αN$^+$**	C_1	87.78	20.05
										βCOαN-αN$^+$		87.13	19.40

^{a} Relative to the **DB*bh*F**. ^{b} Relative to **DB*bh*FH$^+$**.

 This journal is © The Royal Society of Chemistry 2013

Published on 24 September 2013. Downloaded by University of Western Ontario on 31/10/2014 13:25:59.

distance (147 pm) at the *fjord* region and serves as a transition state for enantiomerization of its C_2 global minimum. Their relative stabilities are governed by a combination of steric and electronic effects. The most stable dibenzofluorenones are **DB*bh*F** and **DB*ah*F** which are among the least sterically strained in their overcrowded regions (Table S2†), whereas the least stable **DB*cg*F** has a short contact distance $H^1\cdots H^{13} = 208$ pm and is non-planar. An estimate of the aromatic stabilization in dibenzofluorenones (*vide infra*) shows that the most stable isomers, **DB*bh*F** and **DB*ah*F**, demonstrate relatively low anti-aromaticity of their five-membered rings, as compared with the least stable isomer **DB*cg*F**.

Most of the *O*-protonates of dibenzofluorenones are planar; **DB*ag*FH$^+$**, **DB*ah*FH$^+$** and **DB*ai*FH$^+$** with one benzene ring at [*a*]-position adopt slightly non-planar conformations with the naphthalene dihedral angle $\Phi = 3$–$7°$ (Table S3†), thus avoiding short distances between the hydroxyl and the *peri*-aromatic hydrogen. **DB*cg*FH$^+$**, like **DB*cg*F**, is considerably twisted, $\Phi = 27°$, with a somewhat short contact distance $H^1\cdots H^{13} = 211$ pm. The order of the relative stabilities of the *O*-protonates is the same as the one of the respective ketones. The most stable *O*-protonates are planar **DB*bh*FH$^+$** and **DB*ah*FH$^+$** (Table 5), while the least stable one is highly twisted **DB*cg*FH$^+$**. Analogously to neutral dibenzofluorenones, the antiaromaticity of the central five-membered ring in **DB*bh*FH$^+$** and **DB*ah*FH$^+$** is lower than in **DB*cg*FH$^+$** (*vide infra*), suggesting the higher stability of the formers.

In the σ-complexes of dibenzofluorenones (Fig. 6), the aromatic conjugation in one naphthalene system is broken, leaving one naphthalene system and one benzene ring. The energies and selected geometrical parameters of the σ-complexes of dibenzofluorenones are presented in Table S4.† The HOMA indices (*vide infra*) of the σ-complexes of dibenzofluorenones are presented in Fig. 6. These σ-complexes may be divided into three groups on the basis of their stabilities and HOMA indices of the benzene rings.

(i) The σ-complexes with a benzene ring at [*a*]-position (**σ-13*aH*-DB*ah*F$^+$**, **σ-12*bH*-DB*ai*F$^+$** and **σ-13*aH*-DB*ag*F$^+$**) have the lowest relative energies, and their single benzene rings have the highest HOMA indices, 0.89–0.90.

(ii) The σ-complexes with a benzene rings at [*c*]-position (**σ-6*aH*-DB*bg*F$^+$**, **σ-12*aH*-DB*ag*F$^+$** and **σ-6*aH*-DB*cg*F$^+$**) have lower HOMA indices, 0.75–0.76, and high relative energies.

(iii) The σ-complexes with a benzene ring at [*b*]-position (**σ-12*aH*-DB*ah*F$^+$**, **σ-11*aH*-DB*bh*F$^+$** and **σ-7*aH*-DB*bg*F$^+$**) also have high relative energies, and their benzene rings have the lowest HOMA indices, 0.60–0.62.

Thus, the main factor affecting the relative stabilities of the σ-complexes of dibenzofluorenones is the position of the benzannelation of the protonated ring of the fluorenone moiety. The difference between [*a*]- and [*b*]-/[*c*]-annelation may be explained in simple resonance terms. There are seven Kekulé structures (excluding the non-protonated naphthalene system) in the case of [*a*]-annelation, four of them possess an aromatic sextet. There are six Kekulé structures in the case of [*b*]- and [*c*]-annelation, but only two of them possess an aromatic sextet.

Naphthyl naphthoylium ions, shown in Fig. 7, are constitutional isomers of the *O*-protonates and of the σ-complexes of dibenzofluorenones. Their relative energies and selected geometrical parameters are presented in Table S5.† Their designators are based on the positions of the carbonyl group (**αCO** or **βCO**) and of the naphthyl–naphthyl bond (**αN–αN**, **αN–βN**, **βN–αN** or **βN–βN**). They may be formed from the σ-complexes of dibenzofluorenones by breaking the bond between the carbonyl carbon and the sp^3 carbon of a naphthyl moiety. This process leads to rearomatization of the formerly protonated naphthalene system. Naphthyl naphthoylium ions play an important role in Friedel–Crafts acyl rearrangements of

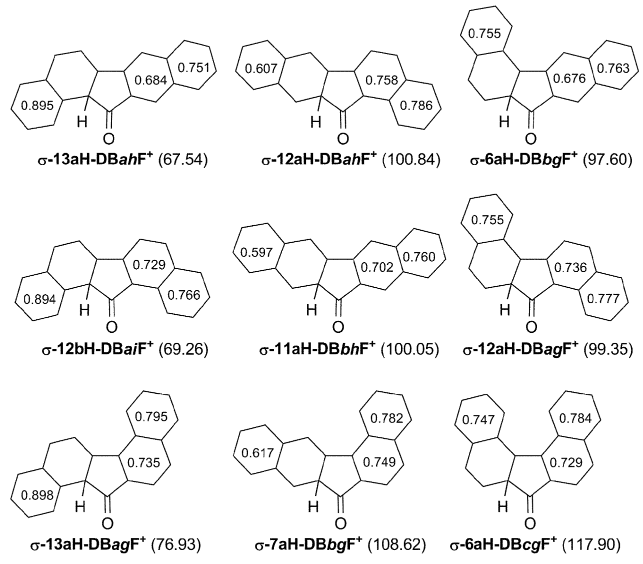

Fig. 6 HOMA indices in σ-complexes of dibenzofluorenones (B3LYP/6-311++G(d,p) free energies (relative to **DB*bh*FH$^+$**) ΔG_{298} in kJ mol^{-1} are given in parentheses; aromatic double bonds are omitted for clarity).

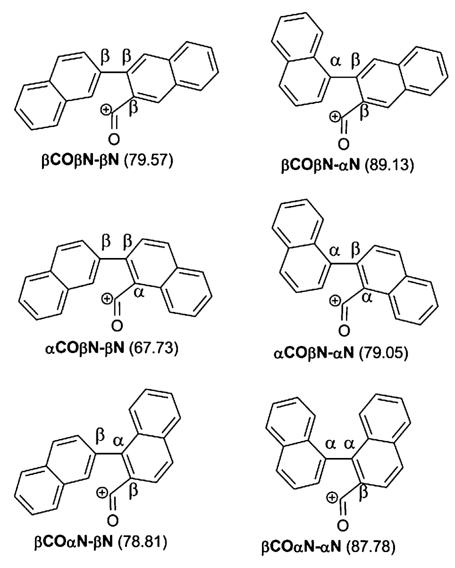

Fig. 7 Naphthyl naphthoylium ions (global minima conformations only, B3LYP/6-311++G(d,p) free energies ΔG_{298}, relative to **DB*bh*FH$^+$**, in kJ mol^{-1} are given in parentheses).

Published on 24 September 2013. Downloaded by University of Western Ontario on 31/10/2014 13:25:59.

dibenzofluorenones (*vide infra*). The most stable of the naphthyl naphthoylium ions is **αCOβN-βN$^+$**, which may be formed from both **σ-12*bH*-DB*ai*F$^+$** and **σ-12*aH*-DB*ah*F$^+$** and serves as an intermediate for the **DB*ai*F ⇌ DB*ah*F** rearrangement. Acylium ion **βCOβN-βN$^+$** may be obtained from both **σ-13*aH*-DB*ah*F$^+$** and **σ-11*aH*-DB*bh*F$^+$** σ-complexes and serves as an intermediate for the **DB*ah*F ⇌ DB*bh*F** rearrangement. Acylium ion **βCOαN-βN$^+$** connects between **σ-13*aH*-DB*ag*F$^+$** and **σ-7*aH*-DB*bg*F$^+$** σ-complexes and, consequently, between **DB*ag*F** and **DB*bg*F**. The remaining naphthyl naphthoylium ions, *i.e.* **αCOβN-αN$^+$**, **βCOαN-αN$^+$** and **βCOβN-αN$^+$** are formed each from a single dibenzofluorenone only (from **σ-12*aH*-DB*ag*F$^+$**, **σ-6*aH*-DB*cg*F$^+$** and **σ-6*aH*-DB*bg*F$^+$**, respectively, see Table S5†) and thus may not participate in the Friedel–Crafts acyl rearrangements.

The energies presented in Table 5 were calculated in the gas phase. In order to test the potential influence of a solvent on the relative energies of the species under study, we have performed solvent reaction field calculations of **DB*ai*F**, **DB*ah*F** and **DB*bh*F**, their *O*-protonates, their σ-complexes and the structurally related naphthyl naphthoylium ions, using the PCM model[42] (Tables S2–S5†). The relative free energies of these species calculated in the presence of water do not differ considerably from the respective energies calculated in gas phase, and show the same order of stabilities: **DB*bh*F** > **DB*ah*F** > **DB*ai*F** for PAKs and their *O*-protonates, **σ-13*aH*-DB*ah*F$^+$** > **σ-12*bH*-DB*ai*F$^+$** > **σ-11*aH*-DB*bh*F$^+$** > **σ-12*aH*-DB*ah*F$^+$** for the σ-complexes.

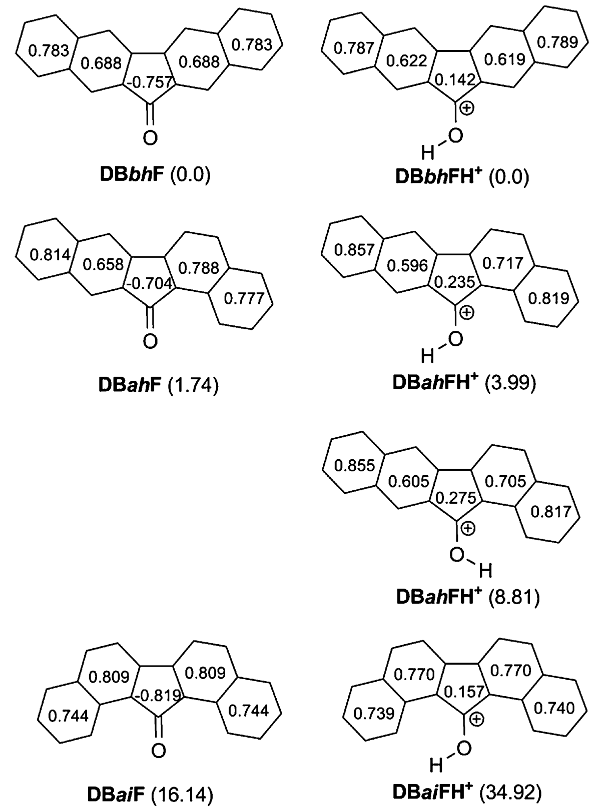

Fig. 8 HOMA indices in selected dibenzofluorenones and their *O*-protonates (B3LYP/6-311G++(d,p) free energies ΔG_{298} in kJ mol^{-1} are given in parentheses).

Aromaticity/antiaromaticity in dibenzofluorenones and their *O*-protonates

The degree of aromatic/antiaromatic stabilization/destabilization in dibenzofluorenones can be estimated by various methods, including HOMA and NICS. HOMA index[43] is a geometry-based index. The HOMA values (in the range of +1 to −1) describe the contribution to the decrease in aromaticity of a cyclic conjugated system due to bond elongation (EN term) and due to bond alternation (GEO term). The HOMA indices of the central five-membered ring and of the 21-membered perimeter of dibenzofluorenones are presented in Table S2.† Fig. 8 shows the B3LYP/6-311G++(d,p) HOMA indices for **DB*ai*F**, **DB*ah*F** and **DB*bh*F**. **DB*bh*F** and **DB*ah*F**, which have the lowest relative energies, possess lower antiaromaticity of their five-membered rings (4πe) as evidenced by their HOMA5 indices (−0.76 and −0.70, respectively). By comparison, **DB*cg*F** has the highest antiaromaticity of its five-membered ring (HOMA5 = −0.84). Analogously, HOMA21 indices (20πe, calculated for the whole 21-membered conjugated systems) of **DB*bh*F** (0.48) and **DB*ah*F** (0.47) are larger than that of **DB*cg*F** (0.41). The HOMA5 indices of dibenzofluorenones demonstrate a strong correlation with their relative Gibbs free energies ΔG_{298}, with Pearson correlation coefficient $\rho = -0.79$. The correlation between the HOMA21 indices, which describe the overall conjugation, and ΔG_{298} values is better, $\rho = -0.92$.

The HOMA indices of the central five-membered ring and of the 21-membered perimeter of the *O*-protonates of dibenzofluorenones are presented in Table S3.† Fig. 8 shows the HOMA indices for the B3LYP/6-311G++(d,p) geometries of **DB*ai*FH$^+$**, **DB*ah*FH$^+$** and **DB*bh*FH$^+$**. The most stable *O*-protonates, **DB*bh*FH$^+$** and **DB*ah*FH$^+$**, exhibit low aromaticity of their five-membered rings (HOMA5 = 0.14 and 0.24). By comparison, the five-membered ring of the least stable **DB*cg*FH$^+$** is non-aromatic (HOMA5 = −0.04). Analogously to dibenzofluorenones, HOMA21 indices of **DB*bh*FH$^+$** and **DB*ah*FH$^+$** are larger than that of **DB*cg*FH$^+$**. HOMA5 and HOMA21 demonstrate a very good correlation with the relative Gibbs free energies ΔG_{298} (ρ = −0.84 and −0.95, respectively).

NICS[44] is a magnetic-based measure of aromaticity which, like HOMA, may be employed to estimate the aromaticity/antiaromaticity of separate rings. NICS values reflect the direction of the ring current in a cyclic conjugated system; they are negative for diamagnetic ring current and positive for the paramagnetic ring current. NICS values of the five-membered rings of dibenzofluorenones and their *O*-protonates are presented in Tables S2 and S3,† respectively. Fig. 9 shows the NICS values in **DB*ai*F**, **DB*ah*F**, **DB*bh*F** and in their respective *O*-protonates. In all the dibenzofluorenones and the *O*-protonates under study, their five-membered rings possess highly positive NICS values, implying the paramagnetic ring current. However, the most stable ketones, **DB*bh*F** and **DB*ah*F**, and *O*-protonates, **DB*bh*FH$^+$** and **DB*ah*FH$^+$**, have the lowest NICS values of their five-membered rings. The NICS values of the five-membered rings demonstrate a strong correlation with the respective free energies ΔG_{298} of dibenzofluorenones and the *O*-protonates, ρ

This journal is © The Royal Society of Chemistry 2013

Published on 24 September 2013. Downloaded by University of Western Ontario on 31/10/2014 13:25:59.

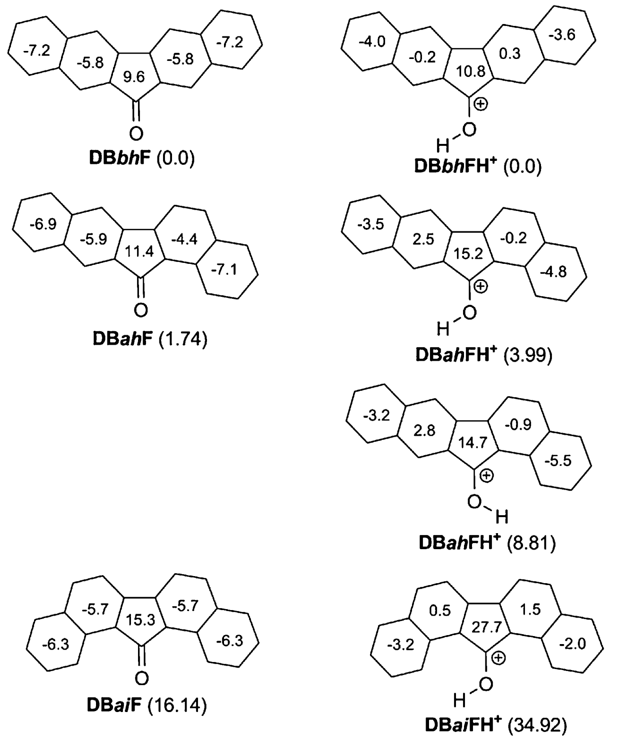

Fig. 9 GIAO//B3LYP/6-311G++(d,p) calculated NICS values in selected dibenzofluorenones and their *O*-protonates.

= 0.98 (excluding **DB*ai*F**, which is an outlier) and 0.90, respectively.

It has not escaped our minds that the *O*-protonates of dibenzofluorenones may be considered antiaromatic. These species may be perceived as hydroxydibenzofluorenium ions (for instance, **DB*ai*FH$^+$** in Fig. 10) and, accordingly, possess an antiaromatic character due to their delocalized $4\pi/20\pi$ electrons ($4n$, $n = 1, 5$). The *O*-protonate of fluorenone has been shown to possess some antiaromatic character and all of its antiaromaticity was found in its five-membered ring.[45] The highly positive NICS values of the five-membered rings in the *O*-protonates are in agreement with the notion of their antiaromaticity. Our NMR spectroscopy results, however, show that the ^{13}C chemical shifts of C=O of these *O*-protonates in trifluoroacetic acid : $CDCl_3$ (19 : 1) as compared with the corresponding shifts in $CDCl_3$ do not indicate a marked effect of antiaromaticity. Moreover, the calculated HOMA indices show, that the five-membered rings in the *O*-protonates of dibenzofluorenones vary from low aromatic to nonaromatic (Table S3†), whereas the five-membered rings in dibenzofluorenones are highly antiaromatic (Table S2†). The HOMA21 indices of the *O*-protonates are also considerably higher than those of dibenzofluorenones, indicating a higher degree of aromaticity of the *O*-protonates. The higher degree of aromaticity in the *O*-protonates as compared to the dibenzofluorenones is attributed to the different charge distribution over the conjugated system. Fig. 11 shows the natural charges in **DB*ai*F**, **DB*ah*F**, **DB*bh*F** and their respective *O*-protonates. Dibenzofluorenones may be considered as dipolar dibenzofluorenylium ions. In **DB*ai*F**, **DB*ah*F** and **DB*bh*F** the partial positive charge (arising due to the contributions of the dipolar structures) is localized mainly in their five-membered rings (+0.27 to +0.40), whereas the benzene rings are nearly devoid of a positive charge (−0.16 to 0.03). In **DB*ai*FH$^+$**, **DB*ah*FH$^+$** and **DB*bh*FH$^+$**, the five-membered rings retain a positive charge (+0.25 to +0.41), but a significant part of the total positive charge is delocalized through the benzene rings, in particular in the terminal ones (+0.11 to +0.15). This

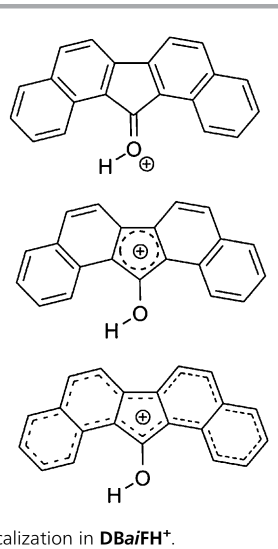

Fig. 10 Electron delocalization in **DB*ai*FH$^+$**.

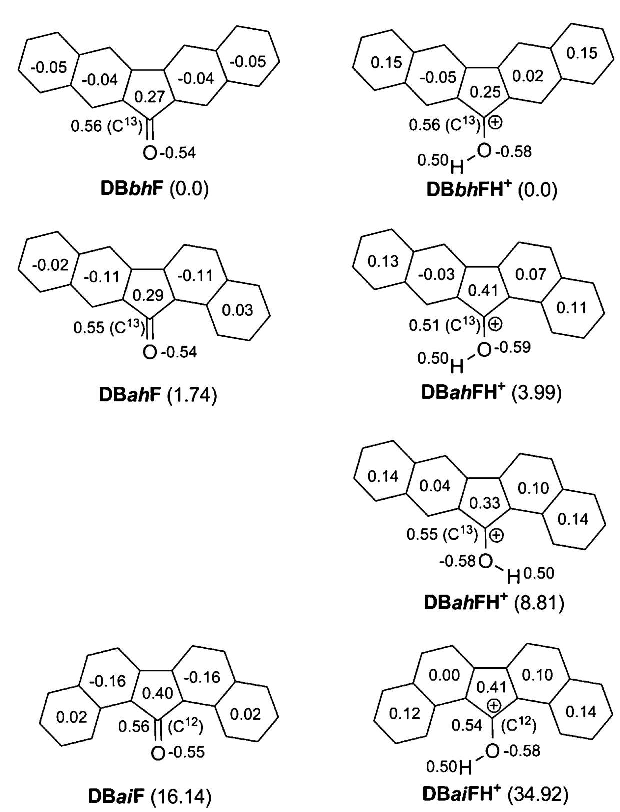

Fig. 11 Natural charges in selected dibenzofluorenones and their *O*-protonates (at B3LYP/6-311G++(d,p), the summation made per each ring).

Published on 24 September 2013. Downloaded by University of Western Ontario on 31/10/2014 13:25:59.

effect is seen even in 9-hydroxyfluorenylium ion (**FlH$^+$**, +0.31 in five-membered ring, +0.23 in six-membered rings) as compared to **Fl** (+0.32 in five-membered ring, 0.02 in six-membered rings).

Dinaphthyl ketones and dibenzofluorenones – structural relationships

The interconnections of the isomers of dibenzofluorenone are presented in Scheme 2. The dibenzofluorenones and their constitutional isomers, depicted in Fig. 1, may be considered as bridged dinaphthyl ketones. Thus, 1,1′-dinaphthyl ketone (**11′DN**), where two naphthyl moieties are connected at their α positions (αα′), is structurally related to **DB*ai*F**, which carries an additional β–β bridge (αα′ + ββ′). 1,2′-Dinaphthyl ketone (**12′DN**), in which two naphthyl moieties are connected at their α and β positions (αβ′), may give rise to two dibenzofluorenones, **DB*ah*F** with an additional β–β bridge (αβ′ + ββ′) and **DB*ag*F** with an additional β–α bridge (αβ′ + βα′). Finally, 2,2′-dinaphthyl ketone (**22′DN**) with (ββ′) connection between its naphthyl moieties may lead to three dibenzofluorenones, **DB*cg*F** (ββ′ + αα′), **DB*bh*F** (ββ′ + ββ′) and **DB*bg*F** (ββ′ + βα′). During the Friedel–Crafts acyl rearrangement the bond between the carbonyl carbon and the sp^3 carbon of a naphthyl moiety is broken. As a result, **DB*ai*F**, **DB*ah*F** and **DB*bh*F** may each mutually undergo acyl rearrangement into other isomers by breaking the αα′, αβ′ or ββ′ bond, respectively, followed by rotation around the remaining ββ′ bond (Scheme 2). Analogously, **DB*ag*F** and **DB*bg*F** may interconvert by breaking the αβ′ or ββ′ bond, respectively, and rotation around the remaining βα′ bond. The sixth dibenzofluorenone, **DB*cg*F**, is not able to undergo an acyl rearrangement to a dibenzofluorenone, due to its naphthyl–naphthyl αα′ bond.

In addition, the structural relationships between the dibenzofluorenones, described above, and their constitutional isomers **DB*ac*F**, **B*hi*C**, **B*de*NC**, **DB*akl*AN** and **B*ij*P** may be considered. **B*hi*C** and **B*ij*P**, like **DB*ai*F**, are structurally related to **11′DN** (αα′), and may be potentially obtained from the latter by forming a bond between β- and *peri*-positions of the naphthyl moieties of **11′DN** (αα′ + β*p*′, leading to **B*hi*C**) or between two *peri*-positions (αα′ + *pp*′, leading to **B*ij*P**). PAKs **DB*akl*AN** and **B*de*NC**, like **DB*ah*F** and **DB*ag*F**, are structurally related to **12′DN** (αβ′), and may be potentially obtained from the latter by forming a bond between α- and *peri*-positions of the naphthyl moieties of **12′DN** (αβ′ + *p*α′, leading to **DB*akl*AN**) or between β and *para*-positions (αβ′ + *p*β′, leading to **B*de*NC**). **DB*ac*F** cannot be formed from any of the dinaphthyl ketones dues to the double annelation at one side of the fluorenone moiety.

Mechanism of Friedel–Crafts acyl rearrangements of dibenzofluorenones

The mechanism of Friedel–Crafts acyl rearrangements proposed above is supported by the results of the DFT calculations (see Tables 5 and S2–S5†). Recently, a computational model for predicting the site for electrophilic aromatic substitution was reported.[46] The model was based on DFT calculations of the relative stabilities of the σ-complex intermediates and was applied (*inter alia*) to Lewis acid promoted Friedel–Crafts acylations. Our calculations give the following orders of relative free energies (ΔG_{298}, kJ mol^{-1}) of **DB*ai*F**, **DB*ah*F**, **DB*bh*F**, **DB*bg*F**, **DB*ag*F** and **DB*cg*F** in each series:

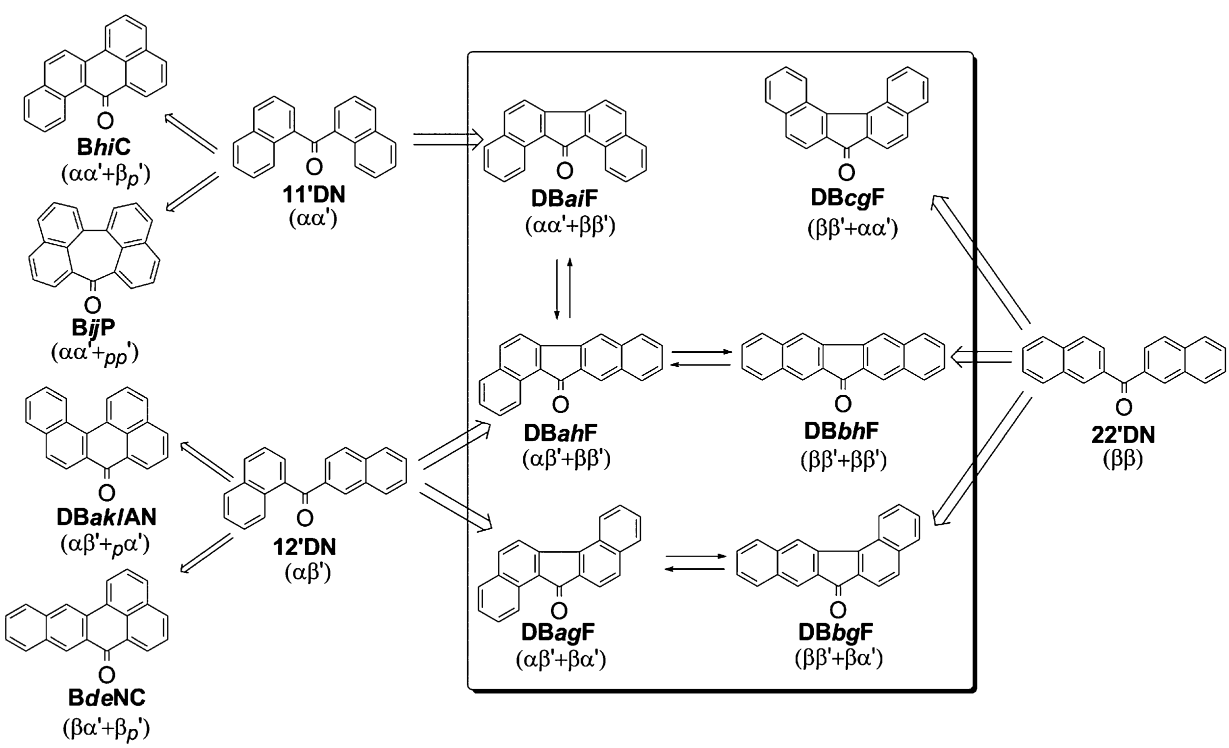

Scheme 2 Structural relationships between dinaphthyl ketones and dibenzofluorenones.

Published on 24 September 2013. Downloaded by University of Western Ontario on 31/10/2014 13:25:59.

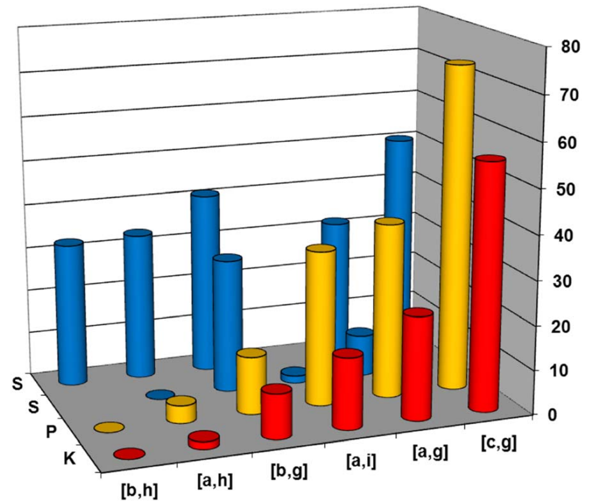

Fig. 12 The B3LYP/6-311++G(d,p) relative free energies ($\Delta\Delta G_{298}$, kJ mol^{-1}) of dibenzofluorenones (**K**), their *O*-protonates (**P**) and σ-complexes (**S**).

• σ-complexes of dibenzofluorenones: $\Delta\Delta G_{298}$ = 0.0 (**σ-13*aH*-DB*ah*F$^+$**), 1.7 (**σ-12*bH*-DB*ai*F$^+$**), 9.4 (**σ-13*aH*-DB*ag*F$^+$**), 30.1 (**σ-6*aH*-DB*bg*F$^+$**), 31.8 (**σ-12*aH*-DB*ag*F$^+$**), 32.5 (**σ-11*aH*-DB*bh*F$^+$**), 33.3 (**σ-12*aH*-DB*ah*F$^+$**), 41.1 (**σ-7*aH*-DB*bg*F$^+$**), 50.4 (**σ-6*aH*-DB*cg*F$^+$**);

• *O*-protonated dibenzofluorenones: ΔG_{298} = 0.0 (**DB*bh*FH$^+$**), 4.0 (**DB*ah*H$^+$**), 13.0 (**DB*bg*FH$^+$**), 34.9 (**DB*ai*FH$^+$**), 39.5 (**DB*ag*FH$^+$**), 73.4 (**Db*cg*FH$^+$**);

• dibenzofluorenones: ΔG_{298} = 0.0 (**DB*bh*F**), 1.7 (**DB*ah*F**), 10.1 (**DB*bg*F**), 16.1 (**DB*ai*F**), 23.4 (**DB*ag*F**), 55.6 (**DB*cg*F**).

Fig. 12 depicts the relative energies of the most stable conformations of each of the dibenzofluorenone species. The B3LYP/6-311++G(d,p) calculated order of stabilities of the σ-complexes of dibenzofluorenones is **σ-13*aH*-DB*ah*F$^+$** ≈ **σ-12*bH*-DB*ai*F$^+$** > **σ-13*aH*-DB*ag*F$^+$** > **σ-6*aH*-DB*bg*F$^+$** ≈ **σ-12*aH*-DB*ag*F$^+$** > **σ-12*aH*-DB*ah*F$^+$** ≈ **σ-11*aH*-DB*bh*F$^+$** > **σ-7*aH*-DB*bg*F$^+$** > **σ-6*aH*-DB*cg*F$^+$**. According to the Hammond–Leffler postulate,[47] the relative energies of the transition states leading to the σ-complexes resemble those of the σ-complexes. Thus, the DFT calculations predict that **DB*ah*F** and **DB*ai*F** are the kinetically controlled products of the Friedel–Crafts acyl rearrangement. By contrast, the calculations show that among the dibenzofluorenones, the linearly dibenzo[*b*]annelated **DB*bh*F** is the most stable, and should be credited as the thermodynamically controlled product. Likewise, among the *O*-protonates of dibenzofluorenones, the linearly dibenzo[*b*]annelated **DB*bh*FH$^+$** is the most stable product. It should be noted, however, that **DB*ah*F** is only slightly less stable than **DB*bh*F**: $\Delta\Delta G_{298}$ = 1.7 kJ mol^{-1} (PAKs), 4.0 kJ mol^{-1} (*O*-protonates). Thus, the DFT calculations support the contention derived from the experimental results that the Friedel–Crafts acyl rearrangements of dibenzofluorenones in PPA are thermodynamically controlled and reversible. The reversible **DB*ah*F** → **DB*ai*F** rearrangement was not observed experimentally, consistently with the low population of **DB*ai*FH$^+$** at equilibrium (ΔG_{413} = 34.3 kJ mol^{-1}).

Conclusions

The dibenzofluorenones under study are planar PAKs (except **DB*cg*F**). The relative stabilities of dibenzofluorenones, their *O*-protonates and σ-complexes are governed by a combination of steric and electronic effects. The reversible pathway of the Friedel–Crafts acyl rearrangements (Agranat–Gore rearrangement[18,20,26]) of dibenzofluorenones established in the present study indicates that non-planarity is not a *sine qua non* condition for the rearrangements. In this case, thermodynamic control wins out over kinetic control, in contrast to the Friedel–Crafts acyl rearrangements in the diacetylanthracene series.[25] The rearrangements are intramolecular. It remains to be seen whether the thermodynamic control is dictated by the intramolecularity of reversible Friedel–Crafts acyl rearrangements.

Experimental

Melting points are uncorrected. NMR spectra were recorded with Bruker Avance II 500 and AMX 400 spectrometers; ^{1}H-NMR spectra were recorded at 500.2 and 400.13 MHz in $CDCl_3$ as a solvent and as an internal standard ($\delta(CHCl_3)$ = 7.260 ppm). ^{13}C-NMR spectra were recorded at 125.78 MHz using $CDCl_3$ as solvent and as internal standard, $\delta(CDCl_3)$ = 77.01 ppm. ^{1}H- and ^{13}C-NMR spectra of *O*-protonates of dibenzofluorenones were recorded using the mixture trifluoroacetic acid (TFA) : $CDCl_3$ (19 : 1) with TFA as an internal standard (δ(TFA) = 11.500 ppm). Complete assignments were made through 2-dimensional correlation spectroscopy (DQF-COSY, HSQC, and HMBC). PPA (84% weight of P_2O_5, dens. 1.9 g mL^{-1}) was purchased from Acros Organics, Israel. Diethyl ether, petroleum ether (40–60 °C, PE), benzene and toluene were dried on sodium.

General procedure for rearrangements of dibenzofluorenones in PPA

In a 150 mL round-bottomed flask equipped with a magnetic stirrer and under argon. PPA was heated for few minutes to the desired temperature. A dibenzofluorenone was then added. The reaction mixture was stirred for desired time at constant temperature. The reaction mixture was then poured into ice water and stirred overnight. The crude products were extracted with CH_2Cl_2, washed with aqueous saturated $NaHCO_3$ and water, and dried over $MgSO_4$. The solvent was evaporated under reduced pressure to give a mixture of isomers (see Table 4) which can be detected and identified according to their ^{1}H-NMR spectra (Table 1).

Synthesis of 13*H*-dibenzo[*ai*]fluoren-13-one (DB*ai*F)

DB*ai*F was prepared by oxidation of dibenzo[*a*,*i*]fluorene with oxygen, using 18-crown-6 ether as a catalyst, in a benzene solution.[48] **DB*ai*F** was obtained as red powder, mp. 269–270 °C (ref. 33, 271–272 °C).

^{1}H-NMR (δ, ppm) 7.406 (dt, J = 8.0 Hz, J = 7.1 Hz, 2H, H^3, H^{10}), 7.573 (dt, J = 8.5 Hz, J = 6.7 Hz, 2H, H^2, H^{11}), 7.655 (dt, J = 8.0 Hz, J = 7.1 Hz, 2H, H^6, H^7), 7.759 (d, J = 8.2 Hz, 2H, H^4, H^9),

Published on 24 September 2013. Downloaded by University of Western Ontario on 31/10/2014 13:25:59.

7.958 (d, J = 8.1 Hz, 2H, H^5, H^8), 8.946 (d, J = 8.4 Hz, 2H, H^1, H^{12}).

^{13}C-NMR (δ, ppm): 117.88 (C^6, C^7), 124.02 (C^1, C^{12}), 126.17 (C^3, C^{10}), 126.76 (C^{13a}, C^{12b}), 128.55 (C^4, C^9), 129.38 (C^2, C^{11}), 130.16 (C^{12a}, C^{13b}), 134.82 (C^{4a}, C^{8a}), 135.25 (C^5, C^8), 145.42 (C^{6a}, C^{6b}), 197.60 (C^{13}).

DB*ai*FH$^+$: ^{1}H-NMR (δ, ppm) 7.39 (t, J = 7.5 Hz, J = 7.7 Hz, 2H, H^3, H^{10}), 7.56 (t, J = 8.4 Hz, 2H, H^2, H^{11}), 7.60 (d, J = 8.1 Hz, 2H, H^6, H^7), 7.74 (d, J = 8.3 Hz, 2H, H^4, H^9), 7.97 (d, J = 8.2 Hz, 2H, H^5, H^8), 8.56 (d, J = 8.7 Hz, 2H, H^1, H^{12}).

^{13}C-NMR (δ, ppm): 120.31 (C^6, C^7), 125.48 (C^1, C^{12}), 128.63 (C^3, C^{10}), 128.94 (C^{13a}, C^{12b}), 131.13 (C^4, C^9), 132.21 (C^2, C^{11}), 132.60 (C^{12a}, C^{13b}), 137.47 (C^{4a}, C^{8a}), 139.06 (C^5, C^8), 148.79 (C^{6a}, C^{6b}), 203.49 (C^{13}).

Synthesis of 13*H*-dibenzo[*ah*]fluoren-13-one (DB*ah*F)

In a 50 mL round bottom flask equipped with magnetic stirrer and under argon, PPA (7.3 g) was added; after stirring for a few minutes at 160 °C, 13*H*-dibenzo[*a*,*i*]fluorenon-13-one (**DB*ah*F**) (0.05 g) was added. The reaction mixture was stirred for 1 h at 160 °C, and then poured into a mixture of ice and water (50 mL). The crude products were extracted with CH_2Cl_2 (2 × 30 mL), washed with saturated aqueous $NaHCO_3$ solution (30 mL) and H_2O (30 mL), and dried over $MgSO_4$. After filtration, the organic solvent was evaporated in vacuum. PLC chromatography on silica gel 60 F_{254} (E. Merck) of the crude products using ethyl acetate : PE (1 : 9), gave a fraction that contained **DB*ah*F**. The compound was extracted with ethyl acetate; the solvent was evaporated under reduced pressure to give **DB*ah*F** as a yellow powder, 0.0127 g; yield 25%, mp. 211.0 °C (ref. 29, 214 °C, ref. 30, 214.0–215.0 °C). Single crystal of **DB*ah*F** was obtained by crystallization from ethyl acetate.

^{1}H-NMR (δ, ppm): 9.128 (d, J = 8.5 Hz, H^1), 8.135 (s, H^{12}), 8.081 (d, J = 8.0 Hz, H^5), 7.909 (d, J = 8.0 Hz, H^{11}), 7.86 (s, H^7), 7.85 (d, J = 8.5 Hz, H^6), 7.85 (d, J = 8.5 Hz, H^8), 7.84 (d, J = 8.5 Hz, H^4), 7.662 (t, J = 7.5 Hz, H^2), 7.560 (t, J = 7.5 Hz, 7.0 Hz, H^9), 7.514 (t, J = 7.5 Hz, 6.5 Hz, H^3), 7.487 (t, J = 7.0 Hz, H^{10}).

^{13}C-NMR (δ, ppm): 194.16 (C^{13}, C=O), 146.54 (C^{6a}), 138.19 (C^{6b}), 136.82 (C^{7a}), 136.27 (C^5), 134.33 (C^{4a}), 134.04 (C^{11a}), 133.53 (C^{12a}), 130.85 (C^{11}), 130.26 (C^{13b}), 129.65 (C^{13a}), 129.51 (C^2), 128.89 (C^9, C^8), 128.55 (C^4), 127.02 (C^{10}), 126.80 (C^3), 125.10 (C^{12}), 124.68 (C^1), 118.92 (C^7), 118.51 (C^6).

LC-MS: m/z = 281 (M^{+1}). IR: ν = 1642.9 cm^{-1} (C=O); UV/Vis ($CHCl_3$, 6.7 × 10^{-6} M, nm): λ = 301, 313, 374, 349sh, 374, 392sh, 473sh.

DB*ah*FH$^+$: ^{1}H-NMR (δ, ppm): 8.64 (d, J = 8.4 Hz, H^1), 7.65 (s, H^{12}), 7.80 (d, J = 8.3 Hz, H^5), 7.60 (d, J = 8.2 Hz, H^4), 7.56 (d, J = 7.0 Hz, H^{11}), 7.55 (d, J = 7.0 Hz, H^8), 7.48 (t, J = 7.6 Hz, H^2), 7.44 (d, J = 8.2 Hz, H^6), 7.43–7.42 (m, H^9), 7.41 (s, H^7), 7.36 (t, J = 8.3 Hz, 7.3 Hz, H^3), 7.32 (t, J = 8.1 Hz, 8.2 Hz, H^{10}).

^{13}C-NMR (δ, ppm): 201.3 (C^{13}, C=O), 150.91 (C^{6a}), 141.01 (C^5), 139.79 (C^{6b}), 139.71 (C^{7a}), 136.89 (C^{4a}), 136.23 (C^{11a}), 134.74 (C^{12a}), 133.43 (C^{11}), 132.70 (C^{13b}), 132.51 (C^2), 132.25 (C^9), 131.30 (C^8), 131.17 (C^4), 131.07 (C^{13a}), 129.88 (C^{10}), 129.41 (C^{12}), 129.35 (C^3), 126.29 (C^1), 122.15 (C^7), 120.57 (C^6).

Synthesis of 7*H*-dibenzo[*cg*]fluoren-7-one (DB*cg*F)

A mixture of [1,1′-binaphthalene]-2,2′-dicarboxylic acid (0.0696 g, 0.20 mmol, prepared from 1-bromo-2-naphthoic acid according to the literature[31]) and acetic anhydride (2.52 mL, 20 mmol) was refluxed for 45 m. Unreacted acetic anhydride, acetic acid and water were removed under reduced pressure, and the solid residue heated at 280 °C for 3 h under argon atmosphere. The resulting red melt was extracted with boiling benzene (3 × 10 mL) and the solvent evaporated, yielding 0.0604 g of red solid. The crude product was purified by sublimation at 5 mm Hg/130 °C, yielding 0.0236 g (41%) of **DB*cg*F** as dark red crystals, mp. 223–224 °C (ref. 31, 222–222.5 °C, ref. 34, 225–226 °C).

^{1}H-NMR (δ, ppm): 8.364 (d, J = 8.2 Hz, H^1), 7.919–7.888 (m, H^4), 7.844 (d, J = 8.0 Hz, H^5), 7.783 (d, J = 8.0 Hz, H^6), 7.605–7.554 (m, H^2, H^3).

^{13}C-NMR (δ, ppm): 194.42 (C^7=O), 146.07 (C^{13b}), 138.84 (C^{4a}), 132.96 (C^{6a}), 130.12 (C^5), 129.33 (C^4), 128.12 (C^{13a}), 127.92 (C^1), 127.75 (C^3), 126.43 (C^2), 119.78 (C^6).

X-ray diffraction study

Single crystal X-ray diffraction was carried out on a Bruker SMART APEX CCD X-ray diffractometer equipped with a graphite-monochromator and using MoK_α radiation (λ = 0.71073 Å). Single crystals were attached to glass fibers, with either epoxy glue, or mineral oil. Data were collected at 173 K. Low temperature was maintained with a Bruker KRYOFLEX nitrogen cryostat. The diffractometer was controlled by a Pentium-based PC running the SMART software package.[49] Immediately after collection, the raw data frames were transferred to a second PC computer for integration and reduction by the SAINT program package.[50] The structures were solved and refined using the SHELXTL software package[51] by full matrix least-squares on F_o^2 with anisotropic displacement parameters for non-hydrogen atoms.

Computational details

The quantum mechanical calculations were performed with the Gaussian09 [52] package. Becke's three-parameter hybrid density functional B3LYP,[53] with the non-local correlation functional of Lee, Yang, and Parr[54] was used. The split valence 6-311++G(d,p) basis set was employed. All structures were fully optimized under the symmetry constraints specified. Vibrational frequencies were calculated to verify the natures of the stationary points. Non-scaled thermal corrections to Gibbs' free energy were used. Natural charges were computed by a full natural orbital analysis, using NBO version 3. NMR shielding tensors were computed with the Gauge-Independent Atomic Orbital method. The calculations in the presence of a solvent (H_2O) were performed using Tomasi's polarized continuum model (PCM),[42] by placing the solute in a cavity within the solvent reaction field, with full geometry optimization of the structures.

 This journal is © The Royal Society of Chemistry 2013

Published on 24 September 2013. Downloaded by University of Western Ontario on 31/10/2014 13:25:59.

Notes and references

1 *Comprehensive Organic Name Reactions and Reagents, Friedel–Crafts Acylation*, ed. Z. Wang, Wiley, 2009, vol. 1, ch. 248, pp. 1126–1130.
2 P. H. Gore, *Chem. Rev.*, 1955, **55**, 229–281.
3 G. A. Olah, *Friedel–Crafts Chemistry*, Wiley-Interscience, New York, 1973, p. 102.
4 C. A. Buehler and D. E. Pearson, *Survey of Organic Synthesis*, Wiley-Interscience, New York, 1970, p. 653.
5 D. E. Pearson and C. A. Buehler, *Synthesis*, 1971, 455–477.
6 P. H. Gore, *Chem. Ind.*, 1974, **18**, 727–731.
7 A. D. Andreou, P. H. Gore and D. F. C. Morris, *J. Chem. Soc., Chem. Commun.*, 1978, 271–272.
8 D. Dowdy, P. H. Gore and D. N. Waters, *J. Chem. Soc., Perkin Trans. 2*, 1991, 1149–1159.
9 I. Agranat, Y.-S. Shih and Y. Bentor, *J. Am. Chem. Soc.*, 1974, **96**, 1259–1260.
10 I. Agranat and Y.-S. Shih, *Synthesis*, 1974, 865–867.
11 I. Agranat and Y.-S. Shih, *Synth. Commun.*, 1974, **4**, 119–126.
12 H. Heaney, The Intramolecular Aromatic Friedel–Crafts Reaction, in *Comprehensive Organic Synthesis*, ed. B. M. Trost, I. Fleming and C. H. Heathcock, Pergamon Press, Oxford, 1991, vol. 2, pp. 753–768.
13 I. Agranat, Y. Bentor and Y.-S. Shih, *J. Am. Chem. Soc.*, 1977, **99**, 7068–7070.
14 M. Frangopol, A. Genunche, P. T. Frangopol and A. T. Balaban, *Tetrahedron*, 1964, **20**, 1881–1888.
15 A. T. Balaban, in *Omagiu Acad. Prof. Raluca Ripan*, ed. C. Dragulesea, Editura Academiei Republicii Socialiste Romania, Bucharest, 1966, pp. 103–109.
16 C. D. Nenitzescu and A. T. Balaban, *Friedel–Crafts and Related Reactions*, ed. G. A. Olah, Wiley-Interscience, New York, 1964, vol. 3, part 2, pp. 1033–1152.
17 F. Effenberger, H. Klenk and P. L. Reiter, *Angew. Chem., Int. Ed. Engl.*, 1973, **12**, 775–776.
18 G. A. Olah, K. Laali and A. K. Mehrotra, *J. Org. Chem.*, 1983, **48**, 3360–3362.
19 L. Levy, S. Pogodin, S. Cohen and I. Agranat, *Lett. Org. Chem.*, 2007, **4**, 314–318.
20 T. Mala'bi, S. Cohen, S. Pogodin and I. Agranat, *Lett. Org. Chem.*, 2009, **6**, 237–241.
21 S. J. J. Titinchi, F. S. Kamounah, H. S. Abbo and O. Hammerich, *ARKIVOC*, 2008, **xiii**, 91–105.
22 C. J. Adams, M. J. Earle, G. Roberts and K. R. Seddon, *Chem. Commun.*, 1998, 2097–2098.
23 A. Okamoto and N. Yonezawa, *Chem. Lett.*, 2009, **38**, 914–915.
24 P. H. Gore, *Friedel–Crafts and Related Reactions*, ed. G. A. Olah, Wiley-Interscience, New York, 1964, vol. 3, part 1, pp. 1–381.
25 T. Mala'bi, S. Pogodin and I. Agranat, *Tetrahedron Lett.*, 2011, **52**, 1854–1857.
26 S. Pogodin, S. Cohen, T. Mala'bi and I. Agranat. Polycyclic Aromatic Ketones – A Crystallographic and Theoretical Study of Acetyl Anthracenes, in *Current Trends in X-Ray Crystallography*, ed. A. Chandrasekaran, InTech, 2011, pp. 3–44.
27 N. Assadi, S. Pogodin, S. Cohen and I. Agranat, *Struct. Chem.*, 2012, **23**, 771–790.
28 A. Levy, M. Goldschmidt and I. Agranat, *Lett. Org. Chem.*, 2006, **3**, 579–584.
29 J. Blum, M. Ashkenasy and Y. Pikholtz, *Synthesis*, 1974, 352–353.
30 M. Zander and W. H. Franke, *Chem. Ber.*, 1965, **98**, 4033–4035.
31 R. H. Martin, *J. Chem. Soc.*, 1941, 679–685.
32 ESI.†
33 D. G. Morris, S. Higgins, K. S. Ryder, R. A. Howie and K. W. Muir, *Acta Crystallogr., Sect. C: Cryst. Struct. Commun.*, 2000, **56**, 570–571.
34 G. L. Eakins, J. S. Alford, B. J. Tiegs, B. E. Breyfogle and C. J. Stearman, *J. Phys. Org. Chem.*, 2011, **24**, 1119–1128.
35 Y. V. Zefirov, *Crystallogr. Rep.*, 1997, **42**, 111–116; translated from *Kristallografiya*, 1997, **42**, 122–128.
36 G. R. Desiraju and A. Gavezzotti, *Acta Crystallogr., Sect. B: Struct. Crystallogr. Cryst. Chem.*, 1989, **45**, 473–482.
37 F. de Proft and P. Geerlings, *Chem. Rev.*, 2001, **101**, 1451–1464.
38 W. Koch and M. C. Holthausen, *A Chemist's Guide to Density Functional Theory*, Wiley-VCH, Weinheim, 2nd edn, 2001.
39 A. Levy, S. Pogodin, S. Cohen and I. Agranat, *Eur. J. Org. Chem.*, 2007, 5198–5211.
40 S. Pogodin, I. D. Rae and I. Agranat, *Eur. J. Org. Chem.*, 2006, 5059–5068.
41 N. Assadi, S. Pogodin and I. Agranat, *Eur. J. Org. Chem.*, 2011, 6773–6780.
42 S. Miertus and J. Tomasi, *Chem. Phys.*, 1982, **65**, 239–241.
43 T. M. Krygowski and M. K. Cyranski, *Chem. Rev.*, 2001, **101**, 1385–1419.
44 N. S. Mills, *Pure Appl. Chem.*, 2012, **84**, 1101–1112.
45 N. S. Mills, *J. Am. Chem. Soc.*, 1999, **121**, 11690–11696.
46 M. Liljenberg, T. Brinck, B. Herschend, T. Rein, G. Rockwell and M. Svensson, *J. Org. Chem.*, 2010, **75**, 4696–4705.
47 P. Muller, Glossary of Terms Used in Physical Organic Chemistry (IUPAC Recommendations 1994), *Pure Appl. Chem.*, 1994, **66**, 1077–1184.
48 N. Assadi, Naphtholougs Analogues of Bistricyclic Aromatic Enes, M.Sc. Thesis (in Hebrew), The Hebrew University of Jerusalem, 2006.
49 *SMART-NT V5.6*, BRUKER AXS GmbH, D-76181 Karlsruhe, Germany, 2002.
50 *SAINT-NT V5.0*, BRUKER AXS GmbH, D-76181 Karlsruhe, Germany, 2002.
51 *SHELXTL-NT V6.1*, BRUKER AXS GmbH, D-76181 Karlsruhe, Germany, 2002.
52 M. J. Frisch, G. W. Trucks, H. B. Schlegel, G. E. Scuseria, M. A. Robb, J. R. Cheeseman, G. Scalmani, V. Barone, B. Mennucci, G. A. Petersson, H. Nakatsuji, M. Caricato, X. Li, H. P. Hratchian, A. F. Izmaylov, J. Bloino, G. Zheng, J. L. Sonnenberg, M. Hada, M. Ehara, K. Toyota, R. Fukuda, J. Hasegawa, M. Ishida, T. Nakajima, Y. Honda, O. Kitao, H. Nakai, T. Vreven, J. A. Montgomery, Jr, J. E. Peralta, F. Ogliaro, M. Bearpark, J. J. Heyd, E. Brothers, K. N. Kudin, V. N. Staroverov, T. Keith, R. Kobayashi, J. Normand, K. Raghavachari, A. Rendell,

J. C. Burant, S. S. Iyengar, J. Tomasi, M. Cossi, N. Rega, J. M. Millam, M. Klene, J. E. Knox, J. B. Cross, V. Bakken, C. Adamo, J. Jaramillo, R. Gomperts, R. E. Stratmann, O. Yazyev, A. J. Austin, R. Cammi, C. Pomelli, J. W. Ochterski, R. L. Martin, K. Morokuma, V. G. Zakrzewski, G. A. Voth, P. Salvador, J. J. Dannenberg, S. Dapprich, A. D. Daniels, O. Farkas, J. B. Foresman, J. V. Ortiz, J. Cioslowski and D. J. Fox, *Gaussian 09, Revision C.01*, Gaussian, Inc., Wallingford CT, 2010.
53 A. D. Becke, *J. Chem. Phys.*, 1993, **98**, 5648–5652.
54 C. Lee, W. Yang and R. G. Parr, *Phys. Rev. B: Condens. Matter Mater. Phys.*, 1988, **37**, 785–789.

Published on 24 September 2013. Downloaded by University of Western Ontario on 31/10/2014 13:25:59.

This journal is © The Royal Society of Chemistry 2013